Measurements of production and inelastic cross sections for p + C, p + Be, and p + Al at 60 GeV/c and p + C and p + Be at 120 GeV/c

A. Aduszkiewicz,[15] E. V. Andronov,[21] T. Antićić,[3] V. Babkin,[19] M. Baszczyk,[13] S. Bhosale,[10] A. Blondel,[23] M. Bogomilov,[2] A. Brandin,[20] A. Bravar,[23] W. Bryliński,[17] J. Brzychczyk,[12] M. Buryakov,[19] O. Busygina,[18] A. Bzdak,[13] H. Cherif,[6] M. Ćirković,[22] M. Csanad,[7] J. Cybowska,[17] T. Czopowicz,[17] A. Damyanova,[23] N. Davis,[10] M. Deliyergiyev,[9] M. Deveaux,[6] A. Dmitriev,[19] W. Dominik,[15] P. Dorosz,[13] J. Dumarchez,[4] R. Engel,[5] G. A. Feofilov,[21] L. Fields,[24] Z. Fodor,[7,16] A. Garibov,[1] M. Gaździcki,[6,9] O. Golosov,[20] M. Golubeva,[18] K. Grebieszkow,[17] F. Guber,[18] A. Haesler,[23] S. N. Igolkin,[21] S. Ilieva,[2] A. Ivashkin,[18] S. R. Johnson,[26] K. Kadija,[3] E. Kaptur,[14] N. Kargin,[20] E. Kashirin,[20] M. Kiełbowicz,[10] V. A. Kireyeu,[19] V. Klochkov,[6] V. I. Kolesnikov,[19] D. Kolev,[2] A. Korzenev,[23] V. N. Kovalenko,[21] K. Kowalik,[11] S. Kowalski,[14] M. Koziel,[6] A. Krasnoperov,[19] W. Kucewicz,[13] M. Kuich,[15] A. Kurepin,[18] D. Larsen,[12] A. László,[7] T. V. Lazareva,[21] M. Lewicki,[16] K. Łojek,[12] B. Łysakowski,[14] V. V. Lyubushkin,[19] M. Maćkowiak-Pawłowska,[17] Z. Majka,[12] B. Maksiak,[11] A. I. Malakhov,[19] A. Marchionni,[24] A. Marcinek,[10] A. D. Marino,[26] K. Marton,[7] H.-J. Mathes,[5] T. Matulewicz,[15] V. Matveev,[19] G. L. Melkumov,[19] A. O. Merzlaya,[12] B. Messerly,[27] Ł. Mik,[13] G. B. Mills,[25] S. Morozov,[18,20] S. Mrówczyński,[9] Y. Nagai,[26] M. Naskręt,[16] V. Ozvenchuk,[10] V. Paolone,[27] M. Pavin,[4,3] O. Petukhov,[18] R. Płaneta,[12] P. Podlaski,[15] B. A. Popov,[19,4] B. Porfy,[7] M. Posiadała-Zezula,[15] D. S. Prokhorova,[21] D. Pszczel,[11] S. Puławski,[14] J. Puzović,[22] M. Ravonel,[23] R. Renfordt,[6] E. Richter-Wąs,[12] D. Röhrich,[8] E. Rondio,[11] M. Roth,[5] B. T. Rumberger,[26] M. Rumyantsev,[19] A. Rustamov,[1,6] M. Rybczynski,[9] A. Rybicki,[10] A. Sadovsky,[18] K. Schmidt,[14] I. Selyuzhenkov,[20] A. Yu. Seryakov,[21] P. Seyboth,[9] M. Słodkowski,[17] A. Snoch,[6] P. Staszel,[12] G. Stefanek,[9] J. Stepaniak,[11] M. Strikhanov,[20] H. Ströbele,[6] T. Šuša,[3] A. Taranenko,[20] A. Tefelska,[17] D. Tefelski,[17] V. Tereshchenko,[19] A. Toia,[6] R. Tsenov,[2] L. Turko,[16] R. Ulrich,[5] M. Unger,[5] F. F. Valiev,[21] D. Veberič,[5] V. V. Vechernin,[21] A. Wickremasinghe,[27] Z. Włodarczyk,[9] A. Wojtaszek-Szwarc,[9] K. Wójcik,[14] O. Wyszyński,[12] L. Zambelli,[4] E. D. Zimmerman,[26] and R. Zwaska[24]

(NA61/SHINE Collaboration)

[1]*National Nuclear Research Center, Baku, Azerbaijan*
[2]*Faculty of Physics, University of Sofia, Sofia, Bulgaria*
[3]*Ruđer Bošković Institute, Zagreb, Croatia*
[4]*LPNHE, University of Paris VI and VII, Paris, France*
[5]*Karlsruhe Institute of Technology, Karlsruhe, Germany*
[6]*University of Frankfurt, Frankfurt, Germany*
[7]*Wigner Research Centre for Physics of the Hungarian Academy of Sciences, Budapest, Hungary*
[8]*University of Bergen, Bergen, Norway*
[9]*Jan Kochanowski University in Kielce, Poland*
[10]*Institute of Nuclear Physics, Polish Academy of Sciences, Cracow, Poland*
[11]*National Centre for Nuclear Research, Warsaw, Poland*
[12]*Jagiellonian University, Cracow, Poland*
[13]*AGH—University of Science and Technology, Cracow, Poland*
[14]*University of Silesia, Katowice, Poland*
[15]*University of Warsaw, Warsaw, Poland*
[16]*University of Wrocław, Wrocław, Poland*
[17]*Warsaw University of Technology, Warsaw, Poland*
[18]*Institute for Nuclear Research, Moscow, Russia*
[19]*Joint Institute for Nuclear Research, Dubna, Russia*
[20]*National Research Nuclear University (Moscow Engineering Physics Institute), Moscow, Russia*
[21]*St. Petersburg State University, St. Petersburg, Russia*
[22]*University of Belgrade, Belgrade, Serbia*
[23]*University of Geneva, Geneva, Switzerland*
[24]*Fermilab, Batavia, Illinois, USA*
[25]*Los Alamos National Laboratory, Los Alamos, New Mexico, USA*
[26]*University of Colorado, Boulder, Colorado, USA*
[27]*University of Pittsburgh, Pittsburgh, Pennsylvania, USA*

This paper presents measurements of production cross sections and inelastic cross sections for the following reactions: 60 GeV/c protons with C, Be, Al targets and 120 GeV/c protons with C and Be targets. The analysis is performed using the NA61/SHINE spectrometer at the CERN Super Proton Synchrotron. First measurements are obtained using protons at 120 GeV/c, while the results for protons at 60 GeV/c are compared with previously published measurements. These interaction cross section measurements are critical inputs for neutrino flux prediction in current and future accelerator-based long-baseline neutrino experiments.

I. INTRODUCTION

Long-baseline neutrino beams are typically initiated by high-energy protons that strike a long target, yielding hadrons that can decay to neutrinos or can reinteract in the target (carbon and beryllium being the most frequently used materials) or in the aluminum focusing horns, potentially producing additional neutrino-yielding hadrons. The NA61/SPS Heavy Ion and Neutrino Experiment (NA61/SHINE) [1], which is a fixed-target experiment at the CERN Super Proton Synchrotron (SPS), has already been very successful at measuring the yields of secondary hadrons generated by protons at 31 GeV/c on carbon targets [2–4] for the T2K long-baseline neutrino oscillation experiment [5]. NA61/SHINE has recently completed data collection at higher energies to benefit other accelerator-based long-baseline neutrino experiments, particularly experiments that use the NuMI beam line or the future LBNF beam line at Fermilab. NuMI is initiated by 120 GeV/c protons on a carbon target, while LBNF will use 60–120 GeV/c protons on a carbon target.

NA61/SHINE has already measured integrated cross sections of pions and kaons to constrain predictions of the neutrino flux coming from reinteractions of pions and kaons [6]. This paper presents measurements of proton integrated cross sections to further improve neutrino flux predictions coming from the primary interactions in the neutrino beam targets or reinteractions of protons in the target and aluminum horns.

During the 2016 data collection, NA61/SHINE recorded interactions of protons on thin carbon, beryllium, and aluminum targets using beam momenta of 60 and 120 GeV/c. Interactions were recorded with all three targets at 60 GeV/c, while interactions on thin carbon and beryllium targets were recorded at 120 GeV/c.

The methodology to measure the inelastic cross section σ_{inel} and the production cross section σ_{prod} follows the same approach as the previous NA61/SHINE measurements [6]. The inelastic process is defined as the sum of all strong-interaction processes that result in the disintegration of the target nucleus (including quasielastic interactions). This is equivalent to the total cross section minus the coherent elastic cross section. The production process is defined as that in which new hadrons are produced. Using the coherent elastic cross section, σ_{el}, and the quasielastic cross section, σ_{qe}, one can define σ_{inel} and σ_{prod} as

$$\sigma_{inel} = \sigma_{total} - \sigma_{el}, \tag{1}$$

$$\sigma_{prod} = \sigma_{inel} - \sigma_{qe}. \tag{2}$$

It is worth noting that not all measurements and experiments use the same terminology for these processes. For instance, the MINERνA experiment [7] at NuMI uses the term "absorption" cross section for σ_{inel}, while previous measurements sometimes refer to either σ_{prod} or σ_{inel} with the term absorption cross section (e.g., Carroll *et al.* [8] used σ_{prod} as the absorption cross section, while Denisov *et al.* [9] used σ_{inel} as the absorption cross section).

II. EXPERIMENTAL SETUP

NA61/SHINE receives a secondary hadron beam from the 400 GeV/c SPS proton beam. Upstream of the NA61/SHINE detector, a magnet system is used to select the desired beam momentum between 13 and 350 GeV/c.

The NA61/SHINE detector [1] is shown in Fig. 1. It comprises two superconducting magnets, five time projection chambers (TPCs), a time-of-flight (TOF) system, and a forward hadron calorimeter (the Projectile Spectator Detector). Two of the TPCs, vertex TPC 1 (VTPC-1) and vertex TPC 2 (VTPC-2), are contained within superconducting magnets capable of generating a combined maximum bending power of 9 T · m. The most critical systems for integrated cross section measurements are the trigger system and the beam position detectors (BPDs). The trigger system uses two scintillator counters (S1 and S2) to trigger on beam particles and two annular scintillation counters ($V0$ and $V1$) to veto divergent beam particles upstream of the target. The 1 cm radius S4 scintillator sits downstream of the target and is used to determine whether or not an interaction has occurred.
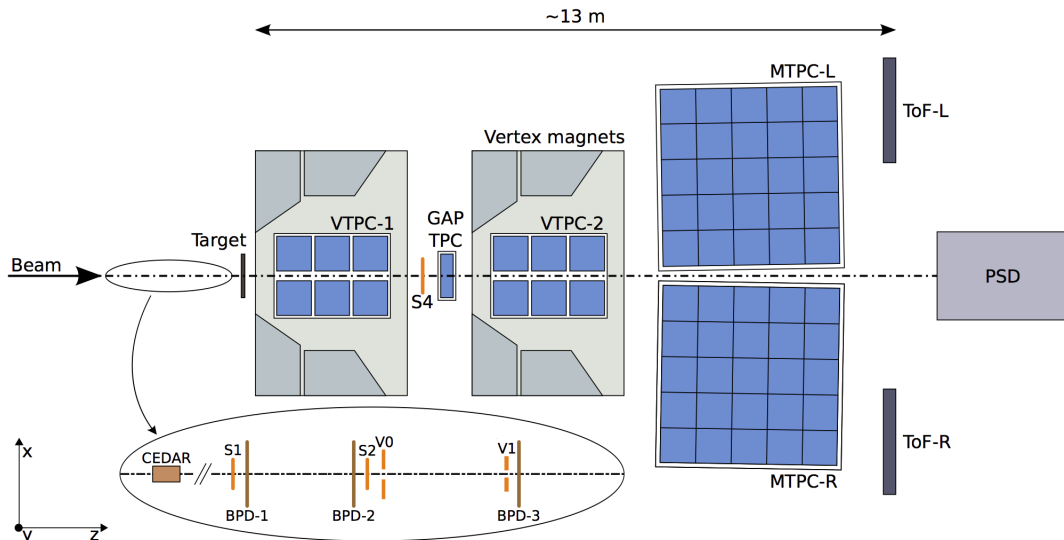
FIG. 1.   The schematic top-view layout of the NA61/SHINE experiment in the configuration used during the 2016 data taking.

A Cherenkov differential counter with achromatic ring focus (CEDAR) [10,11] selects beam particles of the desired species. For the 2016 data at 60 GeV/c (120 GeV/c), the beam was composed of approximately 22% (40%) protons.

Beam particles are selected by defining the beam trigger (T_{beam}) as the coincidence of $S1 \wedge S2 \wedge \overline{V0} \wedge \overline{V1} \wedge$ $CEDAR$. The interaction trigger (T_{int}) is defined by the coincidence of $T_{\text{beam}} \wedge \overline{S4}$ to select beam particles which have interacted with the target. A correction factor for interactions that result in an S4 hit will be discussed in detail in Sec. V A. Three BPDs, which are proportional wire chambers, are located 30.39, 9.09, and 0.89 m upstream of the target and determine the trajectory of the incident beam particle to an accuracy of approximately 100 μm.

Two types of carbon targets were used: one composed of graphite of a density of $\rho = 1.84$ g/cm^3 with dimensions of 25 mm (W) × 25 mm (H) × 20 mm (L) for the 60 GeV/c proton beam, corresponding to roughly 4.2% of a proton-nuclear interaction length, and one composed of graphite of a density of $\rho = 1.80$ g/cm^3 with dimensions of 25 mm (W) × 25 mm (H) × 14.8 mm (L) for the 120 GeV/c proton beam, corresponding to roughly 3.1% of a proton-nuclear interaction length. The former is the same graphite target as was used for past NA61/SHINE measurements, while the latter is a newly produced target using the same type of graphite as the NuMI target. The beryllium target has a density of $\rho = 1.85$ g/cm^3 with dimensions of 25 mm (W) × 25 mm (H) × 14.9 mm (L), corresponding to roughly 3.5% of a proton-nuclear interaction length. This beryllium target is a newly produced target. The aluminum target has a density of $\rho = 2.70$ g/cm^3 with dimensions of 25 mm (W) × 25 mm (H) × 14.8 mm (L), corresponding to roughly 3.6% of a proton-nuclear

interaction length. This aluminum target is the same target as was used for past NA61/SHINE measurements.

III. EVENT SELECTION

Several cuts were applied to events to ensure the purity of the samples and to control the systematic effects caused by beam divergence. First, the so-called WFA (wave form analyzer) cut was used. The WFA determines the timing of beam particles that pass through the S1 scintillator. If another beam particle passes through the beam line close in time, it could cause a false trigger in the S4. In order to mitigate this effect, a conservative cut of ± 2 μs was applied, ensuring that only one particle is allowed to pass through the S1 in a 4 μs time window.

Beam trajectory measurements are especially important for estimating the effects of beam divergence. To understand these effects, tracks are fitted to the reconstructed BPD clusters, and these tracks are extrapolated to the S4 location. The so-called "good BPD" cut requires that the event includes a cluster in the most-downstream BPD and that a track was successfully fit to the BPDs. Figure 2 shows examples of the resulting BPD extrapolation to the S4. As seen in Fig. 2 (left), a halo of beam particles can miss the S4, mimicking the interaction trigger. To avoid such an effect and also to minimize the effect of the S4 size and position uncertainties, which will be discussed in Sec. VI, a radial cut of 0.75 cm was applied to the tracks extrapolated from the BPDs, as indicated in Fig. 2. After the p + C 60 GeV/c data collection, the S4 position was realigned for other measurements which can also be seen in Fig. 2.

About two-thirds of the data were collected with the target inserted and one-third of the data were collected with the target removed. The number of events remaining after the described selection cuts for the target inserted and removed are shown in Tables I–3 for C, Be, and Al.
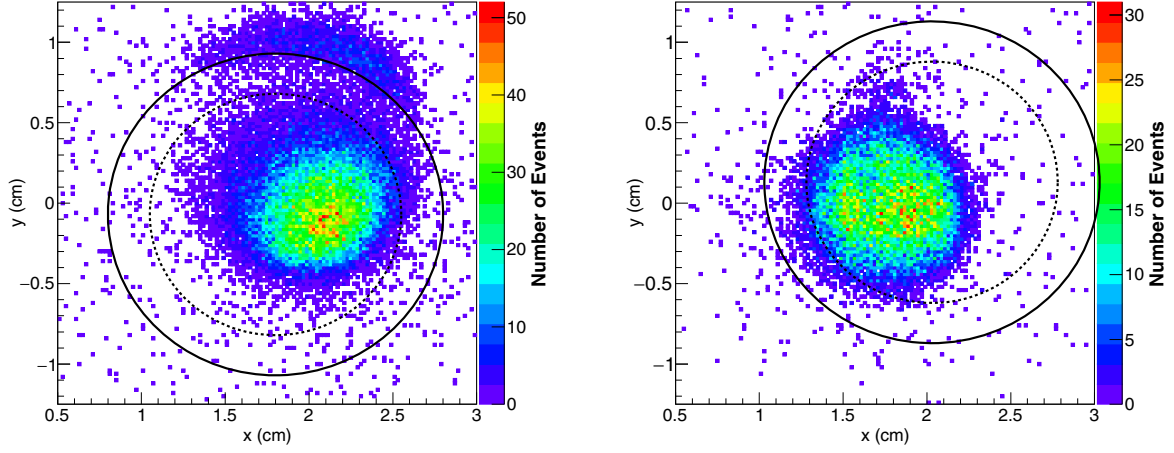
FIG. 2.   Positions of BPD tracks extrapolated to the S4 plane in the target removed data runs from the p + C at 60 GeV/*c* (left) and p + Be at 120 GeV/*c* (right). The measured S4 position is shown as a black circle and the BPD radius cut is shown as a dotted black circle. Events are taken by the interaction trigger defined as T_{int} in Sec. II.

IV. INTERACTION TRIGGER CROSS SECTIONS

The probability of a beam particle interaction inside a thin target is proportional to the thickness, L, and the number density of the target nuclei, n, in the thin target approximation. Thus, the interaction probability, P, can be defined in terms of the interaction cross section, σ:

$$P_{int} = \frac{\text{Number of events}}{\text{Number of beam particles}} = n \cdot L \cdot \sigma. \quad (3)$$

The counts of beam and interaction triggers as described in Sec. II can be used to estimate the trigger probability as follows:

$$P_{\text{Tint}} = \frac{N(T_{\text{beam}} \wedge T_{\text{int}})}{N(T_{\text{beam}})}, \quad (4)$$

where $N(T_{\text{beam}})$ is the number of beam events passing the event selection cuts and $N(T_{\text{beam}} \wedge T_{\text{int}})$ is the number of selected beam events that also have an interaction trigger. In order to correct for events in which the beam particle interacts outside of the target, such as interactions on beam line materials or air, data were also recorded with the target removed from the beam. Table IV summarizes the trigger probabilities for both the target inserted (I) and removed (R) data.

TABLE I.   Number of selected events for p + C at 60 and 120 GeV/*c*.

p + C	60 GeV/*c*		120 GeV/*c*	
Target	Inserted	Removed	Inserted	Removed
Total	254k	116k	393k	217k
WFA	224k	102k	358k	196k
Good BPD	215k	98k	257k	140k
Radial cut	210k	95k	214k	117k

TABLE II.   Number of selected events for p + Be at 60 and 120 GeV/*c*.

p + Be	60 GeV/*c*		120 GeV/*c*	
Target	Inserted	Removed	Inserted	Removed
Total	132k	64k	187k	112k
WFA	119k	58k	173k	103k
Good BPD	67k	33k	108k	64k
Radial cut	65k	31k	104k	62k

TABLE III.   Number of selected events for p + Al at 60 GeV/*c*.

p + Al	60 GeV/*c*	
Target	Inserted	Removed
Total	208k	105k
WFA	188k	94k
Good BPD	117k	58k
Radial cut	113k	57k

TABLE IV.   Trigger probabilities in data. For each configuration, the observed probabilities for target inserted and target removed data are given.

Interaction	$p(\text{GeV}/c)$	$P_{\text{Tint}}^{\text{I}}$	$P_{\text{Tint}}^{\text{R}}$
p + C	60	0.0516 ± 0.0005	0.0047 ± 0.0002
p + Be	60	0.0414 ± 0.0008	0.0031 ± 0.0003
p + Al	60	0.0431 ± 0.0006	0.0034 ± 0.0002
p + C	120	0.0320 ± 0.0004	0.0024 ± 0.0001
p + Be	120	0.0362 ± 0.0006	0.0022 ± 0.0002

TABLE V. Correction factors to the nominal MC simulation for the elastic process obtained with QBBC, and for other processes obtained with FTFP_BERT. The right-hand side shows ratios to the nominal MC simulation for a sample used to assess systematic uncertainties; these ratios were obtained using FTFP_BERT for the elastic process and FTF_BIC for other processes. Model uncertainty treatment is further discussed in Sec. VI C.

| Interaction | p (GeV/c) | MC correction factors (nominal) | | | | | | Ratio to nominal (systematic) | | | | | |
		σ_{el} (mb)	f_{el}	σ_{qe} (mb)	f_{qe}	f_{prod}	f_{inel}	σ_{el}	f_{el}	σ_{qe}	f_{qe}	f_{prod}	f_{inel}
p + C	60	66.6	0.308	25.4	0.788	0.973	0.954	1.11	1.00	0.94	1.08	1.00	1.01
p + Be	60	47.7	0.319	22.4	0.782	0.972	0.951	1.14	1.00	0.94	1.12	1.01	1.02
p + Al	60	126.2	0.231	34.9	0.786	0.974	0.958	1.09	1.00	0.95	1.02	1.00	1.00
p + C	120	65.1	0.085	23.3	0.425	0.926	0.877	1.08	1.00	0.96	1.74	1.02	1.06
p + Be	120	48.9	0.072	21.2	0.409	0.925	0.871	1.08	0.99	0.95	1.97	1.03	1.08

Taking into account the trigger probabilities with the target inserted and removed, P_{Tint}^{I} and P_{Tint}^{R}, the interaction probability P_{int} can be obtained as

$$P_{int} = \frac{P_{Tint}^{I} - P_{Tint}^{R}}{1 - P_{Tint}^{R}}. \quad (5)$$

Using Eqs. (3)–(5), the trigger cross section, σ_{trig}, can be written as

$$\sigma_{trig} = -\frac{m_A}{\rho L N_A} \ln(1 - P_{int}), \quad (6)$$

where N_A, ρ, and m_A are Avogadro's number, the material density, and the atomic mass. The detailed calculation is described in Ref. [6].

V. CORRECTION FACTORS

A. S4 trigger correction factors

The trigger cross section comprises interactions where the resulting particles miss the S4 scintillator. But even when there has been an interaction in the target, there is a possibility that a forward-going particle will strike the S4. Moreover, not all elastically scattered beam particles strike the S4. Corrections must be applied to account for these effects. From Eqs. (1) and (2), the trigger cross section can be related to the production and inelastic cross sections with correction factors:

$$\sigma_{prod} = \frac{1}{f_{prod}} (\sigma_{trig} - \sigma_{qe} \cdot f_{qe} - \sigma_{el} \cdot f_{el}) \quad (7)$$

and

$$\sigma_{inel} = \frac{1}{f_{inel}} (\sigma_{trig} - \sigma_{el} \cdot f_{el}). \quad (8)$$

Here, f_{prod}, f_{qe}, and f_{el} are the fractions of production, quasielastic, and elastic events that miss the S4 counter. These correction factors, as well as σ_{qe} and σ_{el}, are estimated from Monte Carlo (MC) simulations.

GEANT4 version 10.4.p03 [12–14] was used to estimate the MC correction factors. The QBBC physics list was used to estimate correction factors relating to elastic events, while the FTFP_BERT physics list was used to estimate correction factors for other events. The resulting MC correction factors are summarized in Table V (nominal).

B. Beam purity

Kaons are the most probable source of contamination for proton beams. In the case of proton beams at 60 and 120 GeV/c, the CEDAR detector has enough power to discriminate protons from other charged particles. The upper limit on kaon contamination was found to be smaller than 0.1% at 120 GeV/c from pressure scans taken of the CEDAR detector and even lower at 60 GeV/c. It was concluded that the beam purity has a negligible impact on integrated cross section measurements and no correction factor was applied.

VI. SYSTEMATIC UNCERTAINTIES

A. Target density

The uncertainty on the target density affects the calculation of σ_{trig} as shown in Eq. (6). The density uncertainty for each target was estimated by calculating the standard deviation of the target densities determined from measurements of the mass and dimensions of the machined target samples. (There were several machined samples fabricated for each target type.) This evaluation led to a 0.69% uncertainty on carbon, 0.19% uncertainty on beryllium, and a 0.29% uncertainty on aluminum, respectively.

B. S4 size and position

Another systematic uncertainty comes from the size and position of the S4 scintillator. The diameter of the S4 has previously been found to have an uncertainty of ±0.40 mm. The S4 position has been determined using BPD tracks extrapolated to the S4 location. A conservative S4 position uncertainty of ±1.0 mm in X and Y coordinates is assigned. In order to propagate these uncertainties to σ_{inel} and σ_{prod}, two additional MC samples with the S4

TABLE VI. Breakdown of systematic uncertainties for production cross section measurements.

				Systematic uncertainties for σ_{prod} (mb)			
Interaction	p (GeV/c)	Density	S4	Total systematic uncertainties	Elastic model	Other model	Total model uncertainties
p + C	60	±1.9	$\pm^{1.8}_{2.2}$	$\pm^{2.6}_{2.9}$	$\pm^{0.0}_{2.2}$	$\pm^{0.2}_{4.3}$	$\pm^{0.2}_{4.8}$
p + Be	60	±0.4	$\pm^{1.0}_{1.4}$	$\pm^{1.1}_{1.5}$	$\pm^{0.0}_{2.2}$	$\pm^{0.0}_{4.7}$	$\pm^{0.0}_{5.2}$
p + Al	60	±1.4	$\pm^{2.6}_{4.9}$	$\pm^{3.0}_{5.1}$	$\pm^{0.0}_{2.6}$	$\pm^{0.2}_{8.0}$	$\pm^{0.2}_{8.4}$
p + C	120	±1.7	$\pm^{1.9}_{3.1}$	$\pm^{2.5}_{3.5}$	$\pm^{0.0}_{0.4}$	$\pm^{0.0}_{12.2}$	$\pm^{0.0}_{12.2}$
p + Be	120	±0.4	$\pm^{1.7}_{1.8}$	$\pm^{1.7}_{1.8}$	$\pm^{0.0}_{0.2}$	$\pm^{0.1}_{14.3}$	$\pm^{0.1}_{14.3}$

TABLE VII. Breakdown of systematic uncertainties for inelastic cross section measurements.

				Systematic uncertainties for σ_{inel} (mb)			
Interaction	p (GeV/c)	Density	S4	Total systematic uncertainties	Elastic model	Other model	Total model uncertainties
p + C	60	±1.9	$\pm^{1.7}_{2.2}$	$\pm^{2.5}_{2.9}$	$\pm^{0.0}_{2.3}$	$\pm^{0.0}_{4.2}$	$\pm^{0.0}_{4.8}$
p + Be	60	±0.5	$\pm^{1.1}_{1.3}$	$\pm^{1.2}_{1.4}$	$\pm^{0.0}_{2.2}$	$\pm^{0.0}_{3.7}$	$\pm^{0.0}_{4.3}$
p + Al	60	±1.4	$\pm^{2.7}_{4.9}$	$\pm^{3.0}_{5.1}$	$\pm^{0.0}_{2.6}$	$\pm^{0.0}_{6.5}$	$\pm^{0.0}_{7.0}$
p + C	120	±1.8	$\pm^{2.0}_{3.2}$	$\pm^{2.7}_{3.7}$	$\pm^{0.0}_{0.4}$	$\pm^{0.0}_{14.1}$	$\pm^{0.0}_{14.1}$
p + Be	120	±0.4	$\pm^{1.9}_{1.8}$	$\pm^{1.9}_{1.8}$	$\pm^{0.0}_{0.3}$	$\pm^{0.2}_{16.0}$	$\pm^{0.2}_{16.0}$

diameter modified and four additional MC samples with the S4 position shifted were generated.

Previous NA61/SHINE analyses have found that S4 inefficiency is negligibly small [2,6] and this analysis also used the same S4 scintillator. The S4 inefficiency is concluded to be less than 0.1% and neither an uncertainty nor a correction relating to the S4 scintillator efficiency is applied to the results.

C. Model uncertainties

Physics model uncertainties on the S4 trigger correction factors were estimated for elastic and other processes separately. GEANT4 version 10.4.p03 has two models for the elastic process: Barashenkov-Glauber-Gribov and Chips. The former is available with the QBBC physics list, is used for the nominal correction, and is the recommended model by GEANT4. The latter is available with other physics lists including FTFP_BERT. In order to estimate the model uncertainties associated with the elastic process, the S4 correction factors f_{el} and σ_{el} were recalculated with FTFP_BERT, and ratios to the nominal MC simulation are shown in Table V (systematic). Additionally, validity of the model uncertainties on σ_{el} for p + C at 60 and 120 GeV/c have been evaluated with former σ_{el} measurements by Bellettini *et al.* at 21.5 GeV/c [15] and Schiz *et al.* at 70 GeV/c [16] and found to be consistent within uncertainty.

The S4 correction factors f_{prod}, f_{inel}, and f_{qe} as well as σ_{qe} were estimated with FTFP_BERT. In order to estimate the model uncertainties associated with these correction factors, the correction factors were recalculated with three additional physics lists: QBBC, QGSP_BERT, and FTF_BIC. Using these additional correction factors, the model dependence of the integrated cross section measurements was studied. As an example, ratios to the nominal MC simulation obtained with FTF_BIC are shown in Table V (systematic).

All systematic uncertainties discussed in this section are summarized in Tables VI and VII for production and inelastic cross section measurements.

VII. RESULTS AND DISCUSSION

Several production cross sections have been measured in this analysis. Statistical, systematic, and physics model

TABLE VIII. Production cross section measurements with the NA61/SHINE data. The central value as well as the statistical (Δ_{stat}), systematic (Δ_{syst}), and model (Δ_{model}) uncertainties are shown. The total uncertainty (Δ_{total}) is the sum of all uncertainties in quadrature. For comparison, ratios to the GEANT4 predictions with FTFP_BERT ($\frac{\sigma_{prod}}{\sigma_{G4}}$) are also shown.

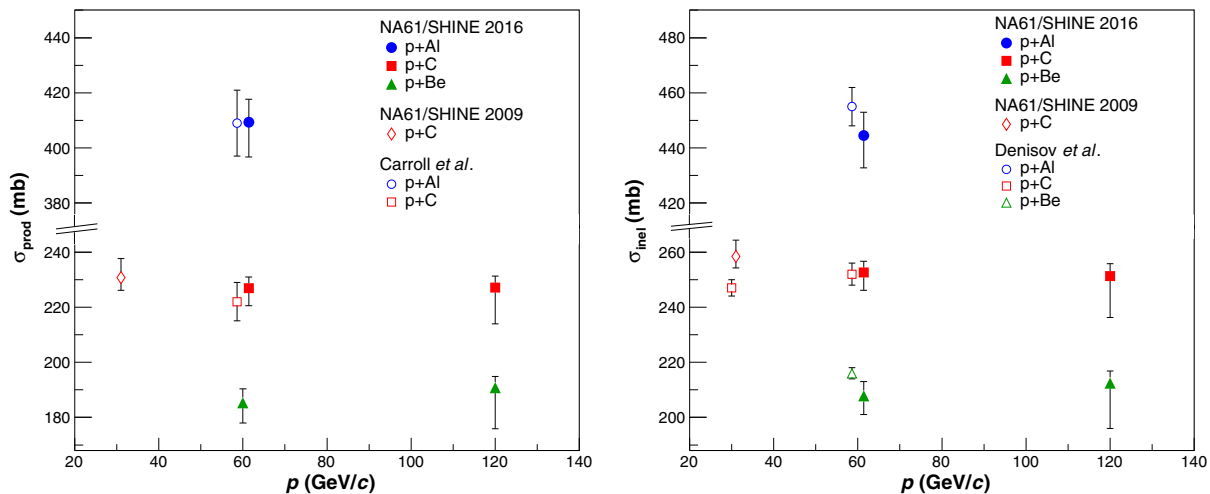|		Production cross section (mb)					
Interaction	p (GeV/c)	σ_{prod}	Δ_{stat}	Δ_{syst}	Δ_{model}	Δ_{total}	$\frac{\sigma_{prod}}{\sigma_{G4}}$
p + C	60	226.9	±3.1	$\pm^{2.6}_{2.9}$	$\pm^{0.2}_{4.8}$	$\pm^{4.1}_{6.4}$	1.05
p + Be	60	185.3	±4.9	$\pm^{1.1}_{1.5}$	$\pm^{0.0}_{5.2}$	$\pm^{5.0}_{7.3}$	1.03
p + Al	60	409.3	±7.8	$\pm^{3.0}_{5.1}$	$\pm^{0.2}_{8.4}$	$\pm^{8.4}_{12.5}$	1.05
p + C	120	227.1	±3.4	$\pm^{2.5}_{3.5}$	$\pm^{0.0}_{12.2}$	$\pm^{4.2}_{13.1}$	1.07
p + Be	120	190.8	±3.7	$\pm^{1.7}_{1.8}$	$\pm^{0.1}_{14.3}$	$\pm^{4.1}_{14.9}$	1.04

FIG. 3. (Left) Summary of production cross section measurements. The results are compared to results by Carroll *et al.* [8]. (Right) Summary of inelastic cross section measurements. The results are compared to results by Denisov *et al.* [9].

uncertainties were estimated separately and are summarized in Table VIII. For comparison, ratios to the GEANT4 10.4.p03 predictions with FTFP_BERT are also shown in Table VIII. Production cross sections were measured to be higher than the predictions of GEANT4. The p + C and p + Al at 60 GeV/c measurements are compared with the results by Carroll *et al.* [8] as shown in Fig. 3 (left). The new NA61/SHINE results are consistent within errors with the previous measurements, and our statistical and systematic uncertainties are smaller.

Several inelastic cross sections have also been determined in this analysis. Statistical, systematic, and physics model uncertainties were estimated separately and are summarized in Table IX. For comparison, ratios to the GEANT4 10.4.p03 predictions with FTFP_BERT are also shown in Table IX. Inelastic cross sections were measured to be higher than the predictions of GEANT4. The measurements with 60 GeV/c protons are compared with the results by Denisov *et al.* [9] in Fig. 3 (right). The

measurements of p + C and p + Al at 60 GeV/c are found to be consistent within errors, while the p + Be at 60 GeV/c inelastic cross section is found to be slightly lower by about 1 standard deviation.

For the proton beam at 120 GeV/c, large GEANT4 physics model dependences were observed. This is due to differences between the correction factors predicted by different physics list, and in particular from FTF_BIC, which has large differences from other physics lists. Differences in these values compared to the nominal values in Table V cause large model uncertainties on nonelastic processes. One possible reason is that the size and position of the S4 scintillator was not optimal for a 120 GeV/c beam. Furthermore, future direct measurements of quasielastic processes will help to reduce model uncertainties, since the measurements presented in this paper have achieved a few % level statistical and systematics uncertainties.

VIII. SUMMARY

In summary, production and inelastic cross sections of protons on carbon, beryllium, and aluminum targets were measured.

The production cross section with a proton beam at 120 GeV/c was measured for the first time with a precision of about 6% (8%) for p + C (p + Be) including statistical, systematic, and model uncertainties. At 60 GeV/c, the measured production cross sections were comparable to previous results for p + C and p + Al, and the precision was improved to about 3%. The production cross section of p + Be at 60 GeV/c was measured for the first time with a precision of about 4% including statistical, systematic, and model uncertainties.

The inelastic cross section with a proton beam at 120 GeV/c was measured for the first time with a precision of about 6% (8%) for p + C (p + Be) including statistical, systematic, and model uncertainties. For the inelastic

TABLE IX. Inelastic cross section measurements with the NA61/SHINE data. The central value as well as the statistical (Δ_{stat}), systematic (Δ_{syst}), and model (Δ_{model}) uncertainties are shown. The total uncertainty (Δ_{total}) is the sum of all uncertainties in quadrature. For comparison, ratios to the GEANT4 predictions with FTFP_BERT ($\frac{\sigma_{inel}}{\sigma_{G4}}$) are also shown.

		Inelastic cross section (mb)				
Interaction	p (GeV/c)	σ_{inel}	Δ_{stat}	Δ_{syst}	Δ_{model}	$\frac{\sigma_{inel}}{\sigma_{G4}}$
p + C	60	252.6	± 3.2	$\pm^{2.5}_{2.9}$	$\pm^{0.0}_{4.8}$	$\pm^{4.1}_{6.5}$	1.05
p + Be	60	207.8	± 5.0	$\pm^{1.2}_{1.4}$	$\pm^{0.0}_{4.3}$	$\pm^{5.1}_{6.7}$	1.03
p + Al	60	444.5	± 7.9	$\pm^{3.0}_{5.1}$	$\pm^{0.0}_{7.0}$	$\pm^{8.5}_{11.7}$	1.05
p + C	120	251.3	± 3.6	$\pm^{2.7}_{3.7}$	$\pm^{0.0}_{14.1}$	$\pm^{4.5}_{15.0}$	1.06
p + Be	120	212.5	± 3.9	$\pm^{1.9}_{1.8}$	$\pm^{0.2}_{16.0}$	$\pm^{4.3}_{16.6}$	1.04

production cross section of the proton beam at 60 GeV/c, reasonable agreement with a previous measurement was found.

The current uncertainties on NuMI and LBNF beam predictions have to extrapolate from data at lower or higher energy than the actual beam energy. Thus, new measurements presented in this paper will improve flux predictions by removing the necessity to extrapolate from different energies.

ACKNOWLEDGMENTS

[1] N. Abgrall *et al.* (NA61/SHINE Collaboration), NA61/SHINE facility at the CERN SPS: Beams and detector system, J. Instrum. **9**, P06005 (2014).

[2] N. Abgrall *et al.* (NA61/SHINE Collaboration), Measurements of $\pi^{\pm}$, $K^{\pm}$, K^0_S, Λ and proton production in proton-carbon interactions at 31 GeV/c with the NA61/SHINE spectrometer at the CERN SPS, Eur. Phys. J. C **76**, 84 (2016).

[3] N. Abgrall *et al.* (NA61/SHINE Collaboration), Measurements of $\pi^{\pm}$ differential yields from the surface of the T2K replica target for incoming 31 GeV/c protons with the NA61/SHINE spectrometer at the CERN SPS, Eur. Phys. J. C **76**, 617 (2016).

[4] N. Abgrall *et al.* (NA61/SHINE Collaboration), Measurements of $\pi^{\pm}$, $K^{\pm}$ and proton double differential yields from the surface of the T2K replica target for incoming 31 GeV/c protons with the NA61/SHINE spectrometer at the CERN SPS, Eur. Phys. J. C **79**, 100 (2019).

[5] K. Abe *et al.* (T2K Collaboration), The T2K experiment, Nucl. Instrum. Methods Phys. Res., Sect. A **659**, 106 (2011).

[6] A. Aduszkiewicz *et al.* (NA61/SHINE Collaboration), Measurements of total production cross sections for π^{+}+C, π^{+}+Al, K^{+}+C, and K^{+}+Al at 60 GeV/c and π^{+}+C and π^{+}+Al at 31 GeV/c, Phys. Rev. D **98**, 052001 (2018).

[7] L. Aliaga *et al.* (MINERvA Collaboration), Design, calibration, and performance of the MINERvA detector, Nucl. Instrum. Methods Phys. Res., Sect. A **743**, 130 (2014).

[8] A. Carroll *et al.*, Absorption cross section of $\pi^{\pm}$, $K^{\pm}$, p and $\bar{p}$ on nuclei between 60 and 280 GeV/c, Phys. Lett. **80B**, 319 (1979).

[9] S. P. Denisov, S. V. Donskov, Yu. P. Gorin, R. N. Krasnokutsky, A. I. Petrukhin, Yu. D. Prokoshkin, and D. A. Stoyanova, Absorption cross sections for pions, kaons, protons and antiprotons on complex nuclei in the 6 to 60 GeV/c momentum range, Nucl. Phys. **B61**, 62 (1973).

[10] C. Bovet, S. Milner, and A. Placci, The Cedar (Cerenkov differential counters with achromatic ring focus) project, IEEE Trans. Nucl. Sci. **25**, 572 (1978).

[11] C. Bovet, R. Maleyran, L. Piemontese, A. Placci, and M. Placidi, The CEDAR counters for particle identification in the SPS secondary beams : A description and an operation manual, CERN Reports No. CERN-82-13 and No. CERN-YELLOW-82-13, 1982.

[12] S. Agostinelli *et al.* (GEANT4 Collaboration), Geant4—a simulation toolkit, Nucl. Instrum. Methods Phys. Res., Sect. A **506**, 250 (2003).

[13] J. Allison *et al.*, Geant4 developments and applications, IEEE Trans. Nucl. Sci. **53**, 270 (2006).

[14] J. Allison *et al.*, Recent developments in GEANT4, Nucl. Instrum. Methods Phys. Res., Sect. A **835**, 186 (2016).

[15] G. Bellettini, G. Cocconi, A. N. Diddens, E. Lillethun, G. Matthiae, J. P. Scanlon, and A. M. Wetherell, Proton-nuclei cross sections at 20 GeV, Nucl. Phys. **79**, 609 (1966).

[16] A. Schiz *et al.*, Hadron-nucleus elastic scattering at 70, 125, and 175 GeV/c, Phys. Rev. D **21**, 3010 (1980).